Magnetic domain wall propagation under ferroelectric control

E. Mikheev,[1] I. Stolichnov,[1] E. De Ranieri,[2] J. Wunderlich,[2] H. J. Trodahl,[3] A. W. Rushforth,[4] S. W. E. Riester,[1]
R. P. Campion,[4] K. W. Edmonds,[4] B. L. Gallagher,[4] and N. Setter[1]

[1]*Ceramics Laboratory, EPFL-Swiss Federal Institute of Technology, Lausanne 1015, Switzerland*
[2]*Hitachi Cambridge Laboratory, JJ Thomson Avenue, Cambridge, CB3 0HE, United Kingdom*
[3]*MacDiarmid Institute for Advanced Materials and Nanotechnology, Victoria University, Wellington, New Zealand*
[4]*School of Physics and Astronomy, University of Nottingham, Nottingham NG7 2RD, United Kingdom*

(Received 11 September 2012; published 19 December 2012)

Control of magnetic domain walls (DWs) and their propagation is among the most promising development directions for future information-storage devices. The well-established tools for such manipulation are the spin-torque transfer from electrical currents and strain. The focus of this paper is an alternative concept based on the nonvolatile ferroelectric field effect on DWs in a ferromagnet with carrier-mediated exchange coupling. The integrated ferromagnet/ferroelectric structure yields two superimposed ferroic patterns strongly coupled by an electric field. Using this coupling, we demonstrate an easy-to-form, stable, nondestructive, and electrically rewritable switch on magnetic domain wall propagation.

DOI: 10.1103/PhysRevB.86.235130 PACS number(s): 75.85.+t, 77.80.Fm, 77.84.Jd

The search for strongly coupled magnetoelectric multiferroics is driven by both the interesting fundamentals and the potential for exploitation in novel spintronic-type devices.[1–3] Of particular practical interest from the device point of view are heterolayered systems with an extrinsic charge-mediated coupling, featuring a ferromagnet with carrier concentration-sensitive properties and a ferroelectric as a source of a nonvolatile field effect. Prominent examples of such combinations are lanthanum manganites with oxide ferroelectrics[4,5] and dilute magnetic semiconductors (DMSs) with polymer ferroelectrics.[6] Closely related is the large body of work using various dielectrics in place of ferroelectrics for volatile control of ferromagnetism in field effect transistor (FET)-like structures.[7–11]

Efforts to date have focused largely on controlling the hysteresis in the ferromagnetic phase, e.g. switching between paramagnetic and ferromagnetic orders,[7,9,10,12] control of magnetization magnitude,[4,9,12] or its coercive field.[6,12] Generally, in the case of charge-driven coupling, the origin of these effects can ultimately be traced to a modulation of the ferromagnetic transition temperature (T_C). It largely tends to be a relatively weak effect limited to a shift of 10–20 K (as in Refs. 4 and 9) or less between the two device states.

A promising, more subtle approach is to switch some further details of the ferromagnetic order. For instance, there have been encouraging results in the attempts to induce magnetization rotation by changing the easy magnetic axis orientation by field effect[13,14] or strain.[15–17] The possibility of strain-mediated control of magnetic domain pattern and DW motion in two-component metal/ferroelectric systems has been demonstrated.[18–20] A volatile electrostatic control of domain wall velocity via a gate dielectric has been achieved in ultrathin cobalt.[21] Such phenomena are also under intense investigation in single-component ferromagnetic systems, such as nanowires of transition metals and dilute magnetic semiconductors, where strain[22–24] and spin-transfer torque[25,26] can be used as manipulation tools. Such control of domain propagation under spin-polarized electrical current pulses is the cornerstone of the racetrack memory concept, which uses DW sequences as memory bits.[27–29]

In this paper, we demonstrate electrostatic control of magnetic domains in a heterolayered DMS/ferroelectric system. Its essential functionality is the possibility to electrically write a reversible and nonvolatile DW propagation switch. This control is unambiguously observed by the strong footprints of DWs in magnetotransport arising from the extraordinary Hall effect (EHE). Moreover, we use the magneto-optical Kerr effect (MOKE) as a direct demonstration, imaging ferromagnetic domain patterns that are controlled by the ferroelectric polarization.

We first present magnetotransport measurements based on the structure illustrated in Fig. 1(a), a ferroelectric-gate FET using a DMS (Mn-doped GaAs) channel.[30] The channel was codoped with phosphorus in order to produce tensile strain in the epitaxial film and thus rotate the easy axis from the common in-plane (IP) to the out-of-plane (OOP) direction.[31–33] As will be seen below, this feature is essential, as it introduces in our system magnetic domain walls[31,34] between the two OOP directions of magnetization M. The ferroelectric gate was formed by the ferroelectric polymer P(VDF-TrFE), whose polarization hysteresis loop is seen in Fig. 1(b). Here, we will show transport data for channels under the remnant polarizations, marked by empty circles. The electric field from the remnant polarization controls the carrier density in the channel, forming stable depletion and accumulation of the holes in the valence band of the channel.[35] The carrier density controls in turn the Mn-Mn exchange, and thus T_C and the properties of the ferromagnetic state of the DMS channel.[36,37]

The EHE is proportional to the perpendicular component of the magnetization vector, yielding the most direct transport signature in the Hall resistance R_{XY} of the (Ga,Mn)(As,P) channel. The response to a magnetic field B applied along the OOP direction was found to be clearly hysteretic below T_C [Fig. 1(c)]. The gate-induced collapse of this hysteresis near T_C (28 K) and the modulation of its coercivity are consistent with its downward (upward) shift in the depletion (accumulation) state of the ferroelectric gate, as reported previously.[6,38]

The data in Fig. 1(c) were obtained on an as-grown channel, in which T_C is suppressed due to carrier compensation by interstitial Mn defects.[36] We have demonstrated previously

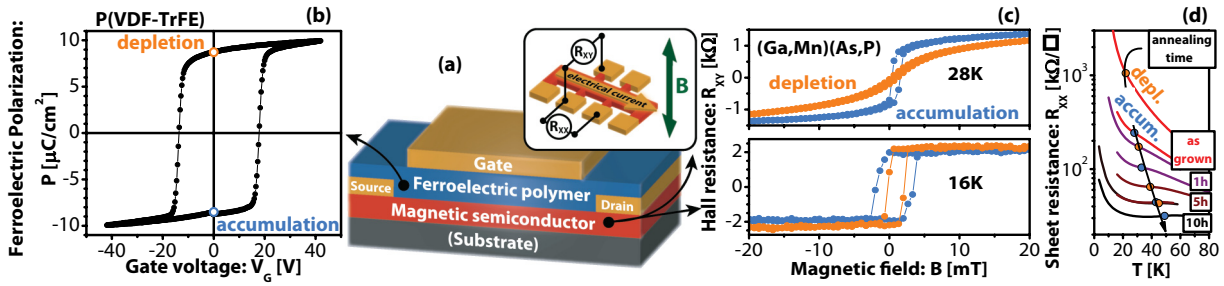

FIG. 1. (Color online) Ferroelectric control of ferromagnetic transition. (a) Schematic of the ferroelectric FET device consisting of a (Ga,Mn)(As,P) dilute magnetic semiconductor channel (DMS) combined with a P(VDF-TrFE) layer forming a polymer ferroelectric gate. The inset illustrates the Hall bar geometry of the DMS channel. (b) Ferroelectric hysteresis loop of P(VDF-TrFE). (c) Extraordinary Hall effect (EHE), as seen in the Hall resistance R_{XY} with magnetic field applied orthogonally to the sample plane. Orange and blue symbols correspond, respectively, to the depletion and accumulation states of the ferroelectric gate. (d) Temperature dependence of the sheet resistance of the DMS channel and its evolution with annealing at 130 °C. Round symbols indicate the ferromagnetic T_C extracted from magnetotransport measurements (see Fig. 2). The orange or blue color of the symbol indicates depletion or accumulation state of the ferroelectric gate.

that T_C can be recovered under a low-temperature annealing regime[38] by removing these interstitial Mn ions from the DMS layer.[39] In this paper, we have focused on the behavior of such structures in which the channel has been annealed at 130 °C for 5 and for 10 h. The recovered high T_C following the annealing process[30] is a direct result of an increase in the carrier (hole) concentration in annealed films, as illustrated by the conductivity data of Fig. 1(d). The gate modulation under depletion/accumulation is, of course, limited in the more heavily doped (annealed) films, but the detection of DW signatures in magnetotransport is greatly simplified.

For an OOP easy axis, the investigation of DW motion is conveniently accomplished by monitoring the Hall (R_{XY}) and longitudinal (R_{XX}) resistances in the geometry shown in Fig. 2(a), with the applied field B now in-plane and parallel to the current I ($B \| I$). The essential advantage of this geometry is that the magnetization reversal process is driven by the very small OOP field component B_Z, due to the experimental misalignment between B and the Hall bar plane [Fig. 2(b)]. The reversal process is then drawn out over a larger applied field range to the point where DW propagation can be examined.

The full sequence of magnetization rotations is readily observed in the measurement of R_{XY} [Fig. 2(c)], which follows the EHE and thus provides a direct measure of the OOP component of M.[40,41] Referring to Fig. 2(c), for a sweep from positive to negative field: At step (I) B is positive and strong enough to force M along the hard axis (IP), resulting in an IP monodomain state. (II) As the field is reduced, M rotates towards its easy axis (OOP). Importantly, M is aligned in one direction by the vertical field component B_Z. (III) As the signs of B and B_Z are reversed, there is a gradual reversal of M towards the opposite OOP direction. (IV) At high negative B, M is once again forced into an IP monodomain state along the IP direction. The following reverse field sweep mirrors these processes.

The presence of domain walls is clearly seen in the longitudinal resistance R_{XX}, which displays asymmetric spikes [Fig. 2(d)] upon magnetization reversal. This signature originates from circulating components of the electrical currents passing through domain walls, leading to the admixture of EHE into the measurement of R_{XX}.[40–43] The spikes thus occur only when there are domain boundaries in the Hall bar, i.e. when the bar is in a multidomain state.

Of particular interest is the step (III) in the magnetization rotation sequence, where the coercive point of R_{XY} signals the absence of a preferential orientation of M. It occurs at the same point in field as the asymmetric spike in R_{XX} and can be interpreted as the point of maximum DW density.[44] The coincidence of these two signatures in our samples is consistently observed over a wide range of temperature and offset angles.[30]

The heavily annealed (Ga,Mn)(As,P) channel of Figs. 2(c) and 2(d) shows unmistakable signatures of the progressive switch between two single-domain states accompanied by domain-wall propagation. However, the ferroelectric control in this channel was limited due to its high hole concentration. In contrast, the much lower hole concentration (and higher resistance) in samples without postgrowth annealing allows for a much higher degree of control [Figs. 2(e) and 2(f)]. This functionality is illustrated by the Hall resistance with $B||I$ in Fig. 2(e). At a temperature of 18 K, the separation between the two reversals of M, signaled by the Hall resistance crossing through zero, is obvious for both the accumulation and depletion polarization. By 24 K, the depletion state shows no opening, confirming that T_C has been exceeded, but in accumulation the hysteretic opening remains even at 28 K. These observations are summarized in Fig. 2(f), which shows this opening plotted vs temperature. The 20% modulation of T_C is the largest we have achieved to date. However, the asymmetric peaks in R_{XX} signaling DW propagation are masked in this channel by its very high electrical resistance.

We turn finally to the intermediate hole concentration film achieved with a 5-h anneal (right-hand section of Fig. 2). At 41 K [Fig. 2(g)], the accumulation state yields a clear hysteresis in the Hall (R_{XY}) resistance, whose coercive point is coincident with a spike in the sheet (R_{XX}) resistance. Both these signatures of magnetization reversal through DW propagation are absent in the depletion state at this temperature, but are recovered at 38 K [upper panel of Fig. 2(g)]. Figure 2(h) has more detailed data[30] for every 0.5 K between 38 and 44 K with R_{XX} peak and R_{XY} crossover fields plotted against temperature. It is clear that the observed

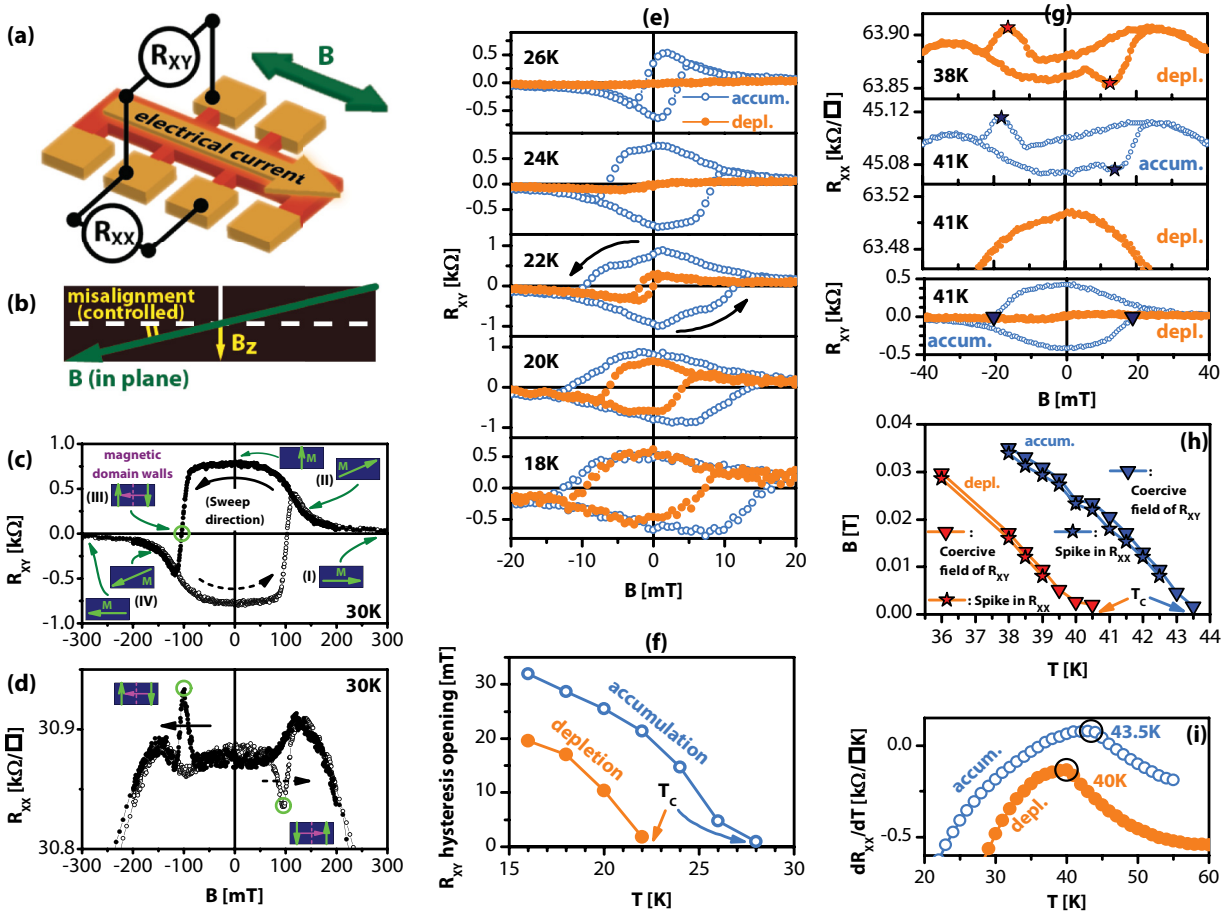

FIG. 2. (Color online) Magnetotransport signatures of magnetic domain walls. (a) Schematic of the magnetotransport geometry with IP applied field. (b) Cross-section view illustrating the small OOP field component B_Z emerging from the experimental misalignment. (c) Resulting sequence of magnetization rotations as seen in R_{XY}, see text for details. The green circle indicates the occurrence of the multidomain state with no preferential orientation of magnetization. The black arrow indicates the direction of B sweep. (d) Parallel measurement of R_{XX}, the two green circles indicate the asymmetric spikes due to magnetic domain walls. (c) and (d) Measurements at $T = 30$ K for a sample annealed for 10 h at 130 °C; (e) and (f) without postprocessing annealing; and (g)–(i) after 5 h at 130 °C. (e) Gated control of the R_{XY} hysteresis near the ferromagnetic T_C. (f) Opening of this hysteresis as a function of T. (g) Situation near T_C, where asymmetric spikes are clearly visible in depletion (38 K, upper panel) and in accumulation (41 K, second panel). At 41 K, poling the gate in depletion induces a disappearance of both the asymmetric spike (third panel) and the R_{XY} hysteresis (bottom panel). (h) Magnetic fields at which the asymmetric spikes in R_{XX} and the coercive points of R_{XY} occur in accumulation and depletion. (i) Cusps of dR_{XX}/dT, indicating T_C.

effect originates from a T_C shift of 3.5 K (8%). Both the absolute value and the shift of T_C observed in this experiment correlate very well with the ones signaled by the cusp in the temperature derivative of sheet resistance dR_{XX}/dT [Fig. 2(i), and Supplemental Material, Fig. 2[30]]. Annealing the device seeks to exploit a tradeoff between the improved clarity of the domain reversal signatures and the reduced temperature gap between accumulation and depletion. Nevertheless, this compromise situation clearly demonstrates the nonvolatile switching of both studied signatures: Coercive point of Hall voltage, indicating magnetization switching, and longitudinal resistance spike characteristic of DW propagation.

We have confirmed the change of ferromagnetic domain dynamics associated with the ferroelectric field effect using magneto-optical polar Kerr effect (MOKE) microscopy. The transparent nature of the polymer ferroelectric gate offers a valuable benefit of optical access, which allows for direct visualization of the ferromagnetic state switching via the MOKE technique. This experiment was carried out on Hall bars fabricated from the same material in the same processing run as the ones used for the transport measurements presented above. These samples were annealed postprocessing for 1 h at 130 °C in order to enhance the measurable MOKE signal.

Prior to placing the samples into the MOKE system, the polarization in the polymer ferroelectric was patterned by applying 30 V to an atomic force microscope (AFM) tip while scanning a region of 50×50 μm, as sketched in Fig. 3(a). The stability and uniformity of the polarization within the poled area have been confirmed by mapping the amplitude and phase of the local piezoelectric response[45] performed 24 h after poling [Figs. 3(b) and 3(c)]. During the MOKE experiments, a perpendicular magnetic field of a few milliTesla (mT) was first applied to the sample in order to induce a fully switched monodomain state. Then the magnetic field direction was reversed and the field was swept by small steps of 0.02 mT to the opposite polarity. After each step, a MOKE image has been

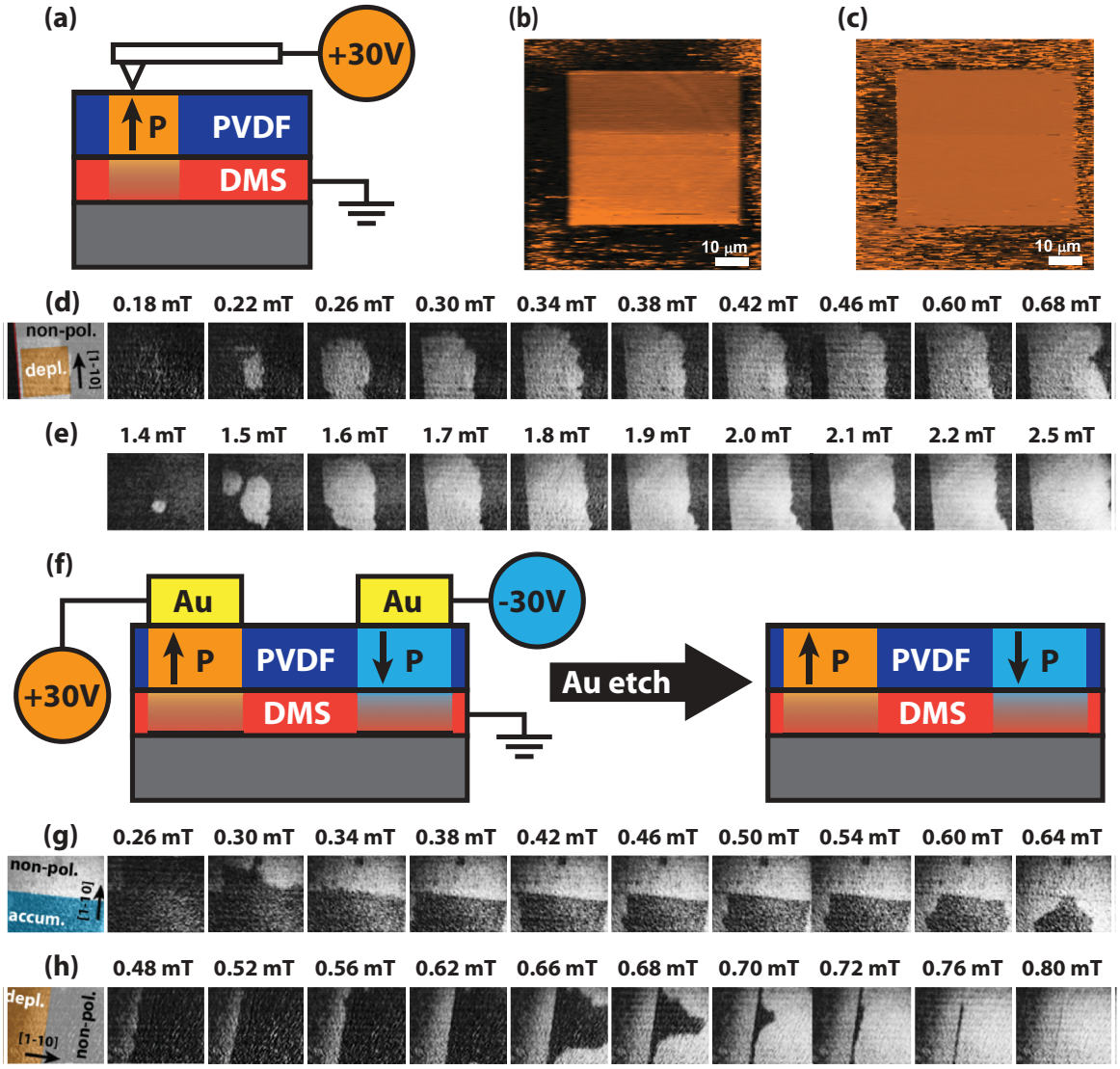

FIG. 3. (Color online) MOKE imaging of magnetic domain propagation controlled by ferroelectric polarization. (a) Schematic of the experiment with ferroelectric patterning by AFM. (b) and (c) Amplitude and phase of the local piezoelectric response of the ferroelectric polymer 24 h after poling of the 50 × 50 μm square in the center of the scanned region. (d) 75 × 100 μm MOKE images for such sample at 31 K (near T_C). The first image illustrates the poled area, with the black arrow indicating the [1-10] crystalline direction of (Ga,Mn)(As,P), the red line neighboring the black region is the edge of the Hall bar. It is followed by a series of MOKE images obtained during a sweep of magnetic field orthogonal to the sample plane. The magnitude of the field is indicated above each frame and the dark (light) regions represent down- (up-) directed magnetization. (e) Same sample at 25 K. (f) Schematic of the experiment with Au electrode removal after poling. (g) MOKE images for the sample poled in accumulation, at 35 K (near T_C). (h) Same as (g) for the sample poled in depletion, at 30 K (near T_C).

collected from the area of 75 × 100 μm covering the border between the poled and nonpoled regions and subtracted from a reference picture in the saturated state.

The resulting differential pictures in Figs. 3(d) and 3(e) and movie 3d in the Supplemental Material[30] clearly show the influence of ferroelectric polarization on the ferromagnetic DW propagation. At 31 K (3–4 K below T_C), the DMS area under the region of the ferroelectric poled by the AFM tip in depletion switches at lower fields compared to the surrounding (unpoled) regions, with multiple nuclei of opposite domains. This observation is fully consistent with a lower T_C and coercive field in depletion state, as expected from the magnetotransport data of Fig. 2. The boundary of the poled ferroelectric area clearly projects on the MOKE images, directly showing that the propagation of the magnetic domains is impeded by this boundary. Similar measurements repeated at 25 K (about 10 K below T_C) demonstrate similar behavior with multiple nucleation sites clearly seen at the initial phase of the switching process. The occurrence of this transient multidomain configuration is in agreement with the appearance of the asymmetric spikes in the longitudinal magnetotransport.

The patterning of the ferroelectric gate was also carried out with an alternative technique, using a standard top gate

electrode for application of a 30 V bias to the ferroelectric gate. After poling, the gold gate electrode was chemically removed by wet etching in order to optically access the channel [Fig. 3(f)]. Ferroelectric patterns obtained with this method induce similar changes in the ferromagnetic domain dynamics. Poling in the accumulation (depletion) state impedes (facilitates) the ferromagnetic switching as shown in the series of images in Figs. 3(g) and 3(h) and movie 3g in the Supplemental Material.[30] In both cases, the boundary of poled/unpoled regions of the polymer gate projects on the magnetic channel as a sharp border between two oppositely magnetized domains. This border remains stable resisting the magnetic domain propagation while the external magnetic field is increased by 0.3–0.35 mT, then a monodomain state gradually sets on. These experiments validate results obtained on the AFM-poled area by showing the same behavior on the areas poled with the conventional electrodes. These data indicate that the change of magnetic properties is a result of the ferroelectric gate effect rather than any alternative mechanism based on magnetic material modification due to the very high electric field in the vicinity of the AFM tip.

The ensemble of Fig. 3 confirms a strong coupling between the superimposed ferroelectric and ferromagnetic domain patterns. By selectively patterning the ferroelectric polarization, one can locally increase or decrease the field threshold for magnetic domain reversal. This can be used to control the direction of DW propagation or to trigger domain nucleation at preferential sites.

Using this gate effect as a tool for manipulation of magnetic domains and DWs is attractive because of its nonvolatile and rewritable nature. This makes it an intriguing complement to the existing concepts of magnetic DW logic using electrical currents to induce their propagation.[27,28] A number of functionalities of interest for such logic can be enabled by the addition of the nonvolatile gate, such as definition of racetrack geometries, particular pinning sites for DWs and voltage switches for closing/opening racetracks for DWs. Moreover, ferroelectric polarization in P(VDF-TrFE) lends itself readily to the definition of complex patterns, including the possibility of lateral downscaling with resolution down to several tens of nanometers.[46] Therefore, while beyond the scope of this work, the DMS/P(VDF-TrFE) system can provide a unique opportunity to study DW dynamics at the nanoscale without the use of lithography.

Coauthors from EPFL acknowledge support from the Swiss National Science Foundation: Project 200020_132724. EU is acknowledged for financial support through the projects ERC-268058 MOBILE-W, COST-0904 and 214499—NAMASTE. AWR acknowledges support from a UK EPSRC Career Acceleration Fellowship (EP/H003487/1).

[1] W. Eerenstein, N. D. Mathur, and J. F. Scott, Nature **442**, 759 (2006).
[2] C. A. F. Vaz, J. Hoffman, C. H. Ahn, and R. Ramesh, Adv. Mater. **22**, 2900 (2010).
[3] C. A. F. Vaz, J. Phys.: Condens. Matter **24**, 333201 (2012).
[4] H. J. A. Molegraaf, J. Hoffman, C. A. F. Vaz, S. Gariglio, D. van der Marel, C. H. Ahn, and J. M. Triscone, Adv. Mater. **21**, 3470 (2009).
[5] C. A. F. Vaz, J. Hoffman, Y. Segal, J. W. Reiner, R. D. Grober, Z. Zhang, C. H. Ahn, and F. J. Walker, Phys. Rev. Lett. **104**, 127202 (2010).
[6] I. Stolichnov, S. W. E. Riester, H. J. Trodahl, N. Setter, A. W. Rushforth, K. W. Edmonds, R. P. Campion, C. T. Foxon, B. L. Gallagher, and T. Jungwirth, Nat. Mater. **7**, 464 (2008).
[7] H. Ohno, D. Chiba, F. Matsukura, T. Omiya, E. Abe, T. Dietl, Y. Ohno, and K. Ohtani, Nature **408**, 944 (2000).
[8] M. Weisheit, S. Fähler, A. Marty, Y. Souche, C. Poinsignon, and D. Givord, Science **315**, 349 (2007).
[9] M. Sawicki, D. Chiba, A. Korbecka, Y. Nishitani, J. A. Majewski, F. Matsukura, T. Dietl, and H. Ohno, Nature Physics **6**, 22 (2009).
[10] Y. Yamada, K. Ueno, T. Fukumura, H. T. Yuan, H. Shimotani, Y. Iwasa, L. Gu, S. Tsukimoto, Y. Ikuhara, and M. Kawasaki, Science **332**, 1065 (2011).
[11] D. Chiba, S. Fukami, K. Shimamura, N. Ishiwata, K. Kobayashi, and T. Ono, Nat. Mater. **10**, 853 (2011).
[12] D. Chiba, M. Yamanouchi, F. Matsukura, and H. Ohno, Science **301**, 943 (2003).
[13] D. Chiba, M. Sawicki, Y. Nishitani, Y. Nakatani, F. Matsukura, and H. Ohno, Nature **455**, 515 (2008).
[14] T. Maruyama, Y. Shiota, T. Nozaki, K. Ohta, N. Toda, M. Mizuguchi, A. A. Tulapurkar, T. Shinjo, M. Shiraishi, S. Mizukami, Y. Ando, and Y. Suzuki, Nature Nanotechnology **4**, 158 (2009).
[15] M. Overby, A. Chernyshov, L. P. Rokhinson, X. Liu, and J. K. Furdyna, Appl. Phys. Lett. **92**, 192501 (2008).
[16] A. W. Rushforth, E. De Ranieri, J. Zemen, J. Wunderlich, K. W. Edmonds, C. S. King, E. Ahmad, R. P. Campion, C. T. Foxon, B. L. Gallagher, K. Výborný, J. Kučera, and T. Jungwirth, Phys. Rev. B **78**, 085314 (2008).
[17] M. Weiler, A. Brandlmaier, S. Geprägs, M. Althammer, M. Opel, C. Bihler, H. Huebl, M. S. Brandt, R. Gross, and S. T. B. Goennenwein, New J. Phys. **11**, 013021 (2009).
[18] T. H. E. Lahtinen, J. O. Tuomi, and S. van Dijken, Adv. Mater. **23**, 3187 (2011).
[19] T. H. E. Lahtinen, K. J. A. Franke, and S. van Dijken, Sci. Rep. **2**, 258 (2012).
[20] D. E. Parkes, S. A. Cavill, A. T. Hindmarch, P. Wadley, F. McGee, C. R. Staddon, K. W. Edmonds, R. P. Campion, B. L. Gallagher, and A. W. Rushforth, Appl. Phys. Lett. **101**, 072402 (2012).
[21] D. Chiba, M. Kawaguchi, S. Fukami, N. Ishiwata, K. Shimamura, K. Kobayashi, and T. Ono, Nature Commun. **3**, 888 (2012).
[22] T.-K. Chung, S. Keller, and G. P. Carman, Appl. Phys. Lett. **94**, 132501 (2009).
[23] T. Brintlinger, S. H. Lim, K. H. Baloch, P. Alexander, Y. Qi, J. Barry, J. Melngailis, L. Salamanca-Riba, I. Takeuchi, and J. Cumings, Nano Lett. **10**, 1219 (2010).

[24]J. Wunderlich, A. C. Irvine, J. Zemen, V. Holý, A. W. Rushforth, E. De Ranieri, U. Rana, K. Výborný, J. Sinova, C. T. Foxon, R. P. Campion, D. A. Williams, B. L. Gallagher, and T. Jungwirth, Phys. Rev. B **76**, 054424 (2007).

[25]M. Yamanouchi, D. Chiba, F. Matsukura, and H. Ohno, Nature **428**, 539 (2004).

[26]M. Hayashi, L. Thomas, R. Moriya, C. Rettner, and S. S. P. Parkin, Science **320**, 209 (2008).

[27]D. A. Allwood, G. Xiong, C. C. Faulkner, D. Atkinson, D. Petit, and R. P. Cowburn, Science **309**, 1688 (2005).

[28]S. S. P. Parkin, M. Hayashi, and L. Thomas, Science **320**, 190 (2008).

[29]G. Catalan, J. Seidel, R. Ramesh, and J. Scott, Rev. Mod. Phys. **84**, 119 (2012).

[30]See Supplemental Material at http://link.aps.org/supplemental/10.1103/PhysRevB.86.235130 for device fabrication details and additional transport and magnetotransport data. Movies 3d and 3g show the whole sequences of 75×100 microns MOKE images partially displayed in Figs. 3(d) and 3(g), respectively. The current magnitude of the magnetic field is shown in the upper left corner.

[31]A. Lemaître, A. Miard, L. Travers, O. Mauguin, L. Largeau, C. Gourdon, V. Jeudy, M. Tran, and J. M. George, Appl. Phys. Lett. **93**, 021123 (2008).

[32]A. W. Rushforth, M. Wang, N. R. S. Farley, R. P. Campion, K. W. Edmonds, C. R. Staddon, C. T. Foxon, and B. L. Gallagher, J. Appl. Phys. **104**, 073908 (2008).

[33]A. Casiraghi, A. W. Rushforth, M. Wang, N. R. S. Farley, P. Wadley, J. L. Hall, C. R. Staddon, K. W. Edmonds, R. P. Campion, C. T. Foxon, and B. L. Gallagher, Appl. Phys. Lett. **97**, 122504 (2010).

[34]S. Haghgoo, M. Cubukcu, H. J. von Bardeleben, L. Thevenard, A. Lemaître, and C. Gourdon, Phys. Rev. B **82**, 041301 (2010).

[35]I. Stolichnov, S. W. E. Riester, E. Mikheev, N. Setter, A. W. Rushforth, K. W. Edmonds, R. P. Campion, C. T. Foxon, B. L. Gallagher, T. Jungwirth, and H. J. Trodahl, Nanotechnology **22**, 254004 (2011).

[36]T. Jungwirth, K. Y. Wang, J. Mašek, K. W. Edmonds, J. König, J. Sinova, M. Polini, N. A. Goncharuk, A. H. MacDonald, M. Sawicki, A. W. Rushforth, R. P. Campion, L. X. Zhao, C. T. Foxon, and B. L. Gallagher, Phys. Rev. B **72**, 165204 (2005).

[37]Y. Nishitani, D. Chiba, M. Endo, M. Sawicki, F. Matsukura, T. Dietl, and H. Ohno, Phys. Rev. B **81**, 045208 (2010).

[38]I. Stolichnov, S. W. E. Riester, E. Mikheev, N. Setter, A. W. Rushforth, K. W. Edmonds, R. P. Campion, C. T. Foxon, B. L. Gallagher, T. Jungwirth, and H. J. Trodahl, Phys. Rev. B **83**, 115203 (2011).

[39]K. W. Edmonds, P. Bogusławski, K. Y. Wang, R. P. Campion, S. N. Novikov, N. R. S. Farley, B. L. Gallagher, C. T. Foxon, M. Sawicki, T. Dietl, M. Buongiorno Nardelli, and J. Bernholc, Phys. Rev. Lett. **92**, 037201 (2004).

[40]G. Xiang, A. W. Holleitner, B. L. Sheu, F. M. Mendoza, O. Maksimov, B. Stone, P. Schiffer, D. D. Awschalom, and N. Samarth, Phys. Rev. B **71**, 241307 (2005).

[41]G. Xiang and N. Samarth, Phys. Rev. B **76**, 054440 (2007).

[42]H. Tang and M. L. Roukes, Phys. Rev. B **70**, 205213 (2004).

[43]X. M. Cheng, S. Urazhdin, O. Tchernyshyov, C. L. Chien, V. I. Nikitenko, A. J. Shapiro, and R. D. Shull, Phys. Rev. Lett. **94**, 017203 (2005).

[44]It is important to note that both these signatures rely on a small misalignment of the field, for which we have carefully maintained a constant offset ($\sim 1^\circ$) in the present experiment to permit direct comparison between the depletion and accumulation measurements.

[45]R. Gysel, I. Stolichnov, A. K. Tagantsev, S. W. E. Riester, N. Setter, G. A. Salvatore, D. Bouvet, and A. M. Ionescu, Appl. Phys. Lett. **94**, 263507 (2009).

[46]B. J. Rodriguez, S. Jesse, S. V. Kalinin, J. Kim, S. Ducharme, and V. M. Fridkin, Appl. Phys. Lett. **90**, 122904 (2007).